Received: 10 May 2021 | Revised: 9 August 2021 | Accepted: 31 August 2021

DOI: 10.1049/ote2.12058

IET Optoelectronics

The Institution of Engineering and Technology WILEY

ORIGINAL RESEARCH PAPER

The BER performance of a FSO system with polar codes under weak turbulence

Nithin Mohan[1] | Zabih Ghassemlooy[1] | Emma Li[1] | Mojtaba Mansour Abadi[1] | Stanislav Zvanovec[2] | Ralph Hudson[3] | Zun Htay[1]

[1]Optical Communications Research Group, Faculty of Engineering and Environment, Northumbria University, Newcastle upon Tyne, UK

[2]Department of Electromagnetic Field, Faculty of Electrical Engineering, Czech Technical University in Prague, Prague, Czech Republic

[3]Tethir Ltd, Newcastle upon Tyne, UK

Correspondence

Nithin Mohan, Optical Communications Research Group, Faculty of Engineering and Environment, Northumbria University, Sutherland Building, Newcastle upon Tyne, NE1 8ST, UK.
Email: nithin.mohan@northumbria.ac.uk

Funding information

MEYS, Grant/Award Number: LTC18008; European Regional Development Fund, Grant/Award Number: 25R17P01847; European Union's COST Action on Newfocus, Grant/Award Number: CA19111

Abstract

The key challenge in free space optical (FSO) communications is combating turbulence-induced fading. As the channel fading in FSO is quasi-static, the transmission parameters such as the code rates, transmit power and modulation schemes can be modified with respect to the channel state information transmitted via the feedback path. As a result, adaptive channel coding is considered as one of the practical approaches to improve the FSO link performance. In this study, the FSO system with polar codes is investigated and its performance is analysed by determining the optimum code-rate required to achieve a bit error rate of 10^{-9} under weak turbulence. It is shown that, using Monte-Carlo simulations for the scintillation indices of 0.12 and 0.2, the successive cancelation list (SCL) decoder offers coding gains of 2.5 and 0.3 dB, respectively, as compared with SC decoder, and for the scintillation index of 0.31, the SC decoder offers a coding gain of 2.5 dB compared to that of the SCL decoder for the code rate.

KEYWORDS

error correction codes, optical communication

1 | INTRODUCTION

The explosive growth in the use of hand-held computing devices has led to a surge in network bandwidth demand, which in turn is putting increasing pressure on the bandwidth usage of current available radio frequency (RF)-based wireless networks. In recent years, free space optical (FSO) communications, as part of the optical wireless system, have emerged as a popular alternative to the RF wireless technologies to overcome the network capacity bottleneck in certain applications, where RF-based link cannot be used, by offering higher data rates, high capacity, inherent security, fast and easy deployment, and a licence free spectrum [1]. These important features make FSO links highly desirable for the provision of high-speed links in the next generation wireless network, including broadcasting, security, wireless front-and back-haul access networks at data rates up to a few 19 Gbps, fibre backup, etc. [1]. However, in outdoor environments, one of the key issues in the intensity modulated/direct detection FSO communication system is the degradation of the links' performance due to the atmospheric conditions such as fog, snow, smoke, and turbulence. The latter, which is due to the inhomogeneity of the temperature and pressure in the atmosphere, results in local variations of the refractive index along the propagation path, leads to the intensity and phase fluctuations of the propagating optical bean, thus leading to fading and beam spreading, and ultimately the link failure [1]. It is to be noted that deep fading can result in severe communication outages. Therefore, to address the limitations of FSO links, several mitigation techniques have been proposed in the literature, such as the aperture averaging [2–4], spatial diversity [5, 6], relay assisted communications [7, 8], adaptive optics [9], and coding [10]. The requirements of synchronisation, high processing complexity and costly implementation are some of the downsides of the proposed mitigation techniques as outlined in [11].

In FSO systems, the channel is assumed to be slowly time variant (i.e., slow fading), where the transmission parameters can be adjusted using the channel state information (CSI). This is provided via a feedback link at the transmitter to improve the quality of the link. In addition, to mitigate turbulence-induced fading and, therefore, improve the links' bit error rate (BER) performance, various error control coding schemes have been proposed and investigated. FSO links with space-time, repetition, and rate-less coding schemes have been reported in the literature [12–14]. A practical scheme of adaptive transmission has been considered to mitigate turbulence-induced fading in FSO links to adjust parameters such as the transmit power, code rates and modulation schemes using the CSI received via the feedback path [11]. Variable and adaptive transmission schemes have been reported in literature [15–19]. In [10], a power allocation scheme in a wavelength division multiplexing (WDM) FSO link was proposed to mitigate atmospheric attenuation. In [16], an adaptive modulation and coding scheme for FSO was proposed where the CSI was estimated at the receiver (Rx) and it relays back to the transmitter (Tx) via an RF feedback path. In [17], a rate adaptive on-off keying FSO link was practically demonstrated using an optimised punctured low-density parity check (LDPC) codes. In [18], a delay and quality-of-service aware adaptive modulation scheme was proposed for a coherent dual-channel optical wireless communication system under Gamma-Gamma (GG) turbulence. In [19], an adaptive transmission system for optical wireless communication using computer-vision techniques is proposed. The computer vision-based multi-domain cooperative adjustment (CV-MDCA) captures on-line images of the communication channel. Features from the processed images are extracted and compared with the standard sample attributes to measure the channel quality index (CQI). The cooperative controller then adjusts various transmission parameters such as encoding, modulation, equalisation, power allocation and information format based on the CQI.

As part of linear codes, polar codes, which are defined using a generator matrix in a recursive manner, offer lower encoding and decoding complexity (i.e., $O(N\log_2(N))$, where N is the code length [20] and O is the big-O notation indicating the performance of the algorithm, and have been used in several applications including relay transmission, multiple access channels, quantum key distributions [20, 21], etc. In the context of FSO communications, the performance of polar codes over the turbulence channel was analysed in [22]. The authors have proposed a CSI evaluation scheme that is utilised to calculate the log-likelihood ratio (LLR) using a 2000-bit pilot sequence, which is the soft-input to the polar decoder. It was experimentally determined that, under weak turbulence, polar codes performed better than LDPC codes; under moderate and strong turbulence using Monte-Carlo simulations, polar codes outperformed LDPC. In [23], the performance of a deep learning-based neural network is investigated under the turbulence regime. Under fixed turbulence conditions, the decoder performance is reported to be stable. In [24], the concept of the polar coded multiple input multiple output (MIMO) FSO communications system is introduced to combat turbulence-induced fading. The MIMO-polar coded system using a successive cancelation list decoder (SCL) offered an improved net coding gain when compared with LDPC with and without spatially correlated fading scenarios.

For finite code lengths, LDPC and turbo codes perform better than those of polar codes, for which several decoding schemes [25, 26] have been proposed to improve the error correcting performance at the cost of increased complexity. In this study, we determine the optimum code-rate R for the scintillation indices σ_I^2 of 0.12, 0.2, and 0.31 for the SC decoder and compare its performance with the SCL decoder under weak turbulence in terms of the BER with the assumption that the channel state information at the Rx is not known. We show that for σ_I^2 of 0.12 and 0.2, the SCL decoder offers coding gains of 2.5 and 0.3 dB, respectively, for the same R over SC decoder, and for σ_I^2 of 0.31, the SC decoder demonstrates improved performance with a coding gain of 2.5 dB for the same R over SCL decoder.

2 | SIGNAL MODEL

In the context of OWC, the received signal is given as follows:

$$y(t) = h(t) * x(t) + n(t), \tag{1}$$

where $h(t)$ is the attenuation due to atmospheric turbulence, $x(t) \in \{0, 1\}$is the transmitted signal, $n(t)$ is the additive white Gaussian noise (AWGN) with zero mean and variance σ_n^2, and $*$ is the convolution operator. A wave traversing in a turbulent channel experiences fading with normalised variance termed as scintillation index, which is given by [27]

$$\sigma_I^2 = \frac{\langle I^2 \rangle - \langle I \rangle^2}{\langle I \rangle^2}, \tag{2}$$

where $\langle \cdot \rangle$ denotes the ensemble average equivalent to long-time averaging with the assumption of an ergodic process, and I is the optical intensity of the propagating wave. From (2), atmospheric turbulence is classified as weak $(\sigma_I^2 < 1)$, moderate $(\sigma_I^2 \cong 1)$, and strong $(\sigma_I^2 > 1)$ [28].

With the assumption of plane wave propagation, σ_I^2 is expressed as [29]

$$\sigma_I^2(D) = \exp\left[\frac{0.49\,\sigma_R^2}{\left(1 + 0.653d^2 + 1.11\sigma_R^{\frac{12}{5}}\right)^{\frac{7}{6}}} + \frac{0.51\,\sigma_R^2\left(1 + 0.69\,\sigma_R^{\frac{12}{5}}\right)^{-\frac{5}{6}}}{\left(1 + 0.9d^2 + 0.621\,d^2\sigma_R^2\right)^{\frac{12}{5}}}\right] - 1, \tag{3}$$

where $d = \frac{D}{2}\sqrt{\frac{k}{l}}$ is the circular aperture scaled by Fresnel zone provided, k is the wavenumber, l is the link length in m, and D is the Rx's aperture diameter. σ_R^2 is the Rytov variance and is expressed as follows:

$$\sigma_R^2 = 1.23 C_n^2 k^{7/6} l^{11/6}, \quad (4)$$

The refractive index parameter C_n^2 has typical values of 10^{-17} and 10^{-13} $\mathrm{m}^{-2/3}$ for the weak and strong turbulence regimes, respectively [29].

For weak turbulence, we consider the log-normal distribution model. The probability density function (PDF) is given as [30]:

$$f_{I_r}(I_r) = \frac{1}{I_r \sigma_I^2(D)\sqrt{2\pi}} \exp\left[-\frac{\left(\ln(I) + \sigma_I^2(D)/2\right)^2}{2\sigma_I^2(D)}\right], \quad (5)$$

where I_r is the normalised irradiance at the receiver. Log-normal distribution serves as a good approximation for turbulence regimes where $\sigma_I^2 < 0.3$ and the average BER for log-normal turbulence is approximately given by [31]

$$P_e \approx \frac{1}{\sqrt{\pi}} \sum_{i=1}^{g} w_i Q\left(\frac{\eta I_0 e^{-2\sigma_x^2 + z_i\sqrt{8\sigma_x^2}}}{\sqrt{2N_0}}\right), \quad (6)$$

where g is the order of approximation, z_i $[i = 1, \ldots, g]$ is the zero of the gth order Hermite polynomial, w_i is the weight factor for the g^{th}-order approximation, I_0 is the optical intensity of the signal devoid of turbulence, $\sigma_x^2 \approx \sigma_I^2/4$ is the log-amplitude fluctuation variance, η is the optical-to-electrical conversion coefficient, and N_0 is the noise power density. For $\sigma_I^2 > 0.3$, the GG turbulence regime is considered and its PDF is given by [30]

$$\frac{2\alpha\beta^2}{\Gamma(\alpha)\Gamma(\beta)} \left(\frac{I}{\langle I \rangle}\right)^{\frac{\alpha+\beta}{2}} K_{\alpha-\beta}\left(2\sqrt{\frac{\alpha\beta I}{\langle I \rangle}}\right), \quad (7)$$

where $K_n(.)$ is the nth order Bessel function of the second kind, and α and β are given by

$$\alpha = \left[\exp\left(\frac{0.49\,\sigma_R^2}{\left(1 + 1.11\sigma_R^{\frac{12}{5}}\right)^{\frac{7}{6}}}\right) - 1\right]^{-1}, \quad (8)$$

$$\beta = \left[\exp\left(\frac{0.51\,\sigma_R^2}{\left(1 + 0.69\,d^2\sigma_R^{\frac{12}{5}}\right)^{\frac{5}{6}}}\right) - 1\right]^{-1}. \quad (9)$$

2.1 | Polar code encoding

Polar codes are capacity achieving codes introduced by Arikan [32]. It provides a low-complexity method to construct polarised channels, where a fraction of noiseless channels tends to the capacity of binary-input discrete memoryless channel (B-DMC). The channel polarisation concept discussed in [32] consists of a transformation, which produces N synthetic bit-channels from N independent copies of B-DMC. The synthetic channels are polarised meaning that bits with different probability of decoding are transmitted. The design of (N, K) polar codes involves the generation of input vector $\mathbf{u} = [u_0, u_1, u_2, \ldots u_{N\text{-}1}]$ by assigning K information bits to the K most reliable channels. The remaining N-K bits form the frozen set and do not carry any information [33]. The codeword $\mathbf{d} = [d_0, d_1, d_2, \ldots, d_{N-1}]$ is computed as follows:

$$\mathbf{d} = \mathrm{u} \times \mathbf{G_N}, \quad (10)$$

where $\mathbf{G_N}$ is the $N \times N$ channel transformation matrix given by

$$\mathbf{G_N} = \mathbf{G}_2^{\otimes n}, \quad (11)$$

where $\mathbf{G}_2 = \begin{bmatrix} 1 & 0 \\ 1 & 1 \end{bmatrix}$ is the transform kernel for 2-bit, $n = \log_2(N) = 1, 2, 3 \ldots$, N is the code length, and $\otimes$ is the Kronecker product.

Figure 1a depicts the encoding mechanism of (8,4) polar code, where the frozen bit set belongs to the bit positions 0, 1, 2, and 4 of $\mathbf{u}$. The message bits are placed in bit positions 3, 5, 6, and 7 of $\mathbf{u}$. Using (7) and (8), $\mathbf{u}$ is encoded to obtain the codeword $\mathbf{d}$.

2.2 | SC and SCL decoders

The SC decoder, which is the most common in polar code, operates as a depth-first binary tree search, see Figure 1b, where each sub-tree is represented as a constituent node. The white and black nodes represent the information and frozen bits, respectively, whereas the grey nodes represent a concatenation of two constituent nodes. More specifically, the Rx observes $\mathbf{y}$ and estimates the elements of $\mathbf{u}$. The decoder finds a sub-optimal solution by maximising the likelihood via a greedy one-time-pass through the tree. The LLR α of each received codeword is passed down from the parent node to the child node, as shown in Figure 1b. Hard-decision estimated β are sent from the child nodes to the parent node. The left branch messages α_l are computed according to the F function using the min-sum approximation as given by [34]

$$\begin{aligned} \alpha_l[i] &= F\left(\alpha[i],\ \alpha\left[i + \frac{N}{2}\right]\right) \\ &\approx \mathrm{sgn}(\alpha[i])\,\mathrm{sgn}\left(\alpha\left[i + \frac{N}{2}\right]\right) \min\left|\left(\alpha[i],\ \alpha\left[i + \frac{N}{2}\right]\right)\right|. \end{aligned} \quad (12)$$

The right branch messages α_r are calculated using the G function as follows:

$$\begin{aligned} \alpha_r[i] &= G\left(\alpha[i],\ \alpha\left[i + \frac{N}{2}\right], \beta_l[i]\right) \\ &= \alpha_v\left[i + \frac{N}{2}\right] - \left(2\beta_l[i] - 1\right)\alpha_v[i]. \end{aligned} \quad (13)$$

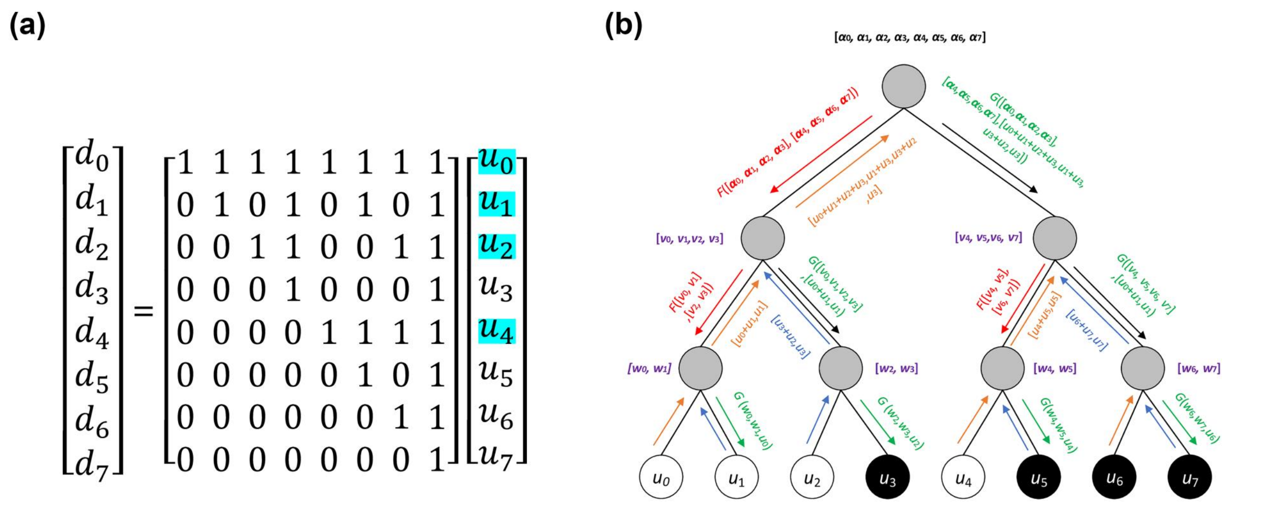

FIGURE 1 (a) (8,4) polar encoding mechanism with frozen bits highlighted in blue, and (b) its corresponding decoder tree

For each codeword received, each node in the tree receives alpha and sends α_l (represented as in red arrows) to the successive node, receives β_l (represented by orange arrows), calculates and sends α_r (represented in blue) based on β_l. After receiving β_l and β_r, β is sent from the node to its parent node. β is computed as follows:

$$\beta[i] = \begin{cases} \beta_l[i] \oplus \beta_r[i], & \text{when } i < \dfrac{N}{2} \\ \beta_r\left[i - \dfrac{N}{2}\right], & \text{otherwise} \end{cases} \tag{14}$$

where $\oplus$ refers to XOR operation and in this context is referred to as *combine* operation.

When a leaf node is encountered, the estimated bit is given as follows:

$$\hat{u}[i] = \begin{cases} 0, & \text{if } i \in F \text{ or } \alpha[i] \geq 0, \\ 1, & \text{otherwise,} \end{cases} \tag{15}$$

where $\mathcal{F}$ represents the frozen bit set. A SC list decoder was proposed in [35] as an improvement over the SC decoder in terms of error correction capability.

SCL decoding, which converts the greedy one-time-pass search of SC decoding into a breadth-first search, follows the same algorithm as SC decoding until the bit information estimation stage at the leaf nodes. For each estimate at the leaf node, both 0 and 1 are considered. This results in a list of $2L$ candidate codewords out of which L-codeword is removed based on the path metric, which is computed for each candidate codeword as [36]

$$\mathrm{PM}_{i_l} = \begin{cases} \mathrm{PM}_{i-1_l}, \text{ if } \hat{u}_{i_l} = \dfrac{1}{2}\left(1 - \mathrm{sgn}\left(\alpha_{i_l}\right)\right) \\ \mathrm{PM}_{i-1_l} + \left|\alpha_{i_l}\right| \quad \text{otherwise,} \end{cases} \tag{16}$$

where l is the path index and $\hat{u}_{i_l}$ is the estimated bit i in l. It is to be noted that the L-path with the lowest PM will survive.

2.3 | LLR computation for on-off keying (OOK) under additive Gaussian noise channel

For OOK, the transmitted symbol is defined as follows:

$$x(t) = \begin{cases} 0, & m(t) = 0 \\ 1, & m(t) = 1 \end{cases}, \tag{17}$$

where $m(t)$ is the message bits. From Bayes' rule, we have

$$P[x(t) = 0 |\, y(t)] = \frac{P[y(t)|x(t) = 0]P[(x(t) = 0]}{P[y(t)]}, \tag{18}$$

$$P\left[x(t) = 1 \middle|\, y(t)\right] = \frac{P[y(t)|x(t) = 1]P(x(t) = 1]}{P[y(t)]}. \tag{19}$$

For the AWGN channel, the received signal and the conditional probability are as given by, respectively [37],

$$y(t) = \begin{cases} 1 + n(t), & \text{if } i\, x(t) = 1 \\ n(t), & \text{if } i\, x(t) = 0 \end{cases}, \tag{20}$$

$$P[y(t)|x(t) = \tau] = \frac{1}{\sqrt{2\pi\sigma}} e^{\frac{-[y(t) - \mu_\tau]^2}{2\sigma_\tau^2}}, \tag{21}$$

where μ_τ and σ_τ are the mean and standard deviation for $\tau = 0$, 1. From (17) to (21), α per bit is computed as follows:

$$\alpha = \ln\left[\frac{P[y(t)|x(t) = 0]}{P[y(t)|x(t) = 1]}\right] = \frac{1 - 2.y(t)}{2\sigma_n^2}. \tag{22}$$

From a practical standpoint, the calculation of the exact LLR following a stochastic model is quite complex [37]. Computation of LLRs could prove to be costly in terms of the computation complexity, hardware area and memory at the channel output [38, 39]. In [39–41], computation of the approximate LLR methods were proposed. In this work, the LLRs for the FSO system are approximated as follows:

$$\alpha \approx 1 - 2 \cdot y(t). \tag{23}$$

Using Monte-Carlo simulations, the BER performance for the link with the SC decoder, given that the noise power is known at the Rx (i.e., true LLR values), and the SC decoder with the approximated LLR as per (23) for the AWGN channel is depicted in Figure 2. It is observed that the decoder performance using the LLR approximation is only slightly inferior to the SC decoder with the true LLR values of 0.2 dB measured at the BER of 10^{-5}, thus resulting in no significant deterioration in the BER performance.

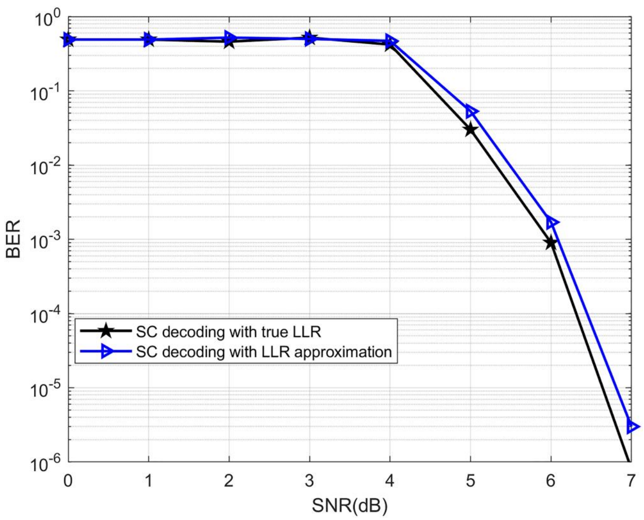

FIGURE 2 Bit error rate performance of true log-likelihood ratio (LLR) with approximated LLR using the SC decoder

2.4 | System model

As shown in Figure 3, a random message bit sequence $\boldsymbol{m}$ in the non-return to zero OOK format is applied to the polar code encoder to generate a fixed length codeword $\boldsymbol{d}$ with N of 1024-bits for intensity modulation of the optical source. The channel follows log-normal and GG distributions for $\sigma_I^2 \leq 0.3$ and >0.3, respectively. Following transmission over the free space channel, the codeword $\boldsymbol{y}$ is received at the optical Rx. Using (20), the LLR of the received signal $\boldsymbol{y}$ is computed and decoded using the SC/SCL decoder to obtain $\boldsymbol{m_{est}}$. Although, narrow transmit beams are preferred in free space optical (FSO) links, for short-range FSO links, wide divergence angle light sources are highly desirable to ease the alignment requirement and therefore compensate for the pointing loss at the cost of increased geometric loss [42]. Typically, the beam divergence is in the range of 2-10 mrad for the non-tracking systems, which translates to a beam spot of 2-10 m for a 1 km link. In this work, we have assumed a beam with a wide divergence for ground-to-train communications as described in [43], which is practical, therefore offsetting the pointing loss at the cost of increased geometric loss [44]. However, for a point-to-point long range FSO link, misalignment must be considered.

From a practical system's perspective, adaptive coding could be considered as a prudent approach to mitigate turbulence/scintillation experienced by the FSO link. The practical implementation of the proposed system can be carried out using purpose-built modules or FPGA, which will involve using the RF link for the feedback signal on channel state information. Alternatively, the adaptive coding part could be readily implemented using software defined radio (SDR), see Figure 4. In the SDR-based transmitter, the message bits are encoded using an adaptive Polar encoder, which adjusts the code rate based on the strength of the turbulence estimated by the CSI estimate block. The CSI is estimated by determining

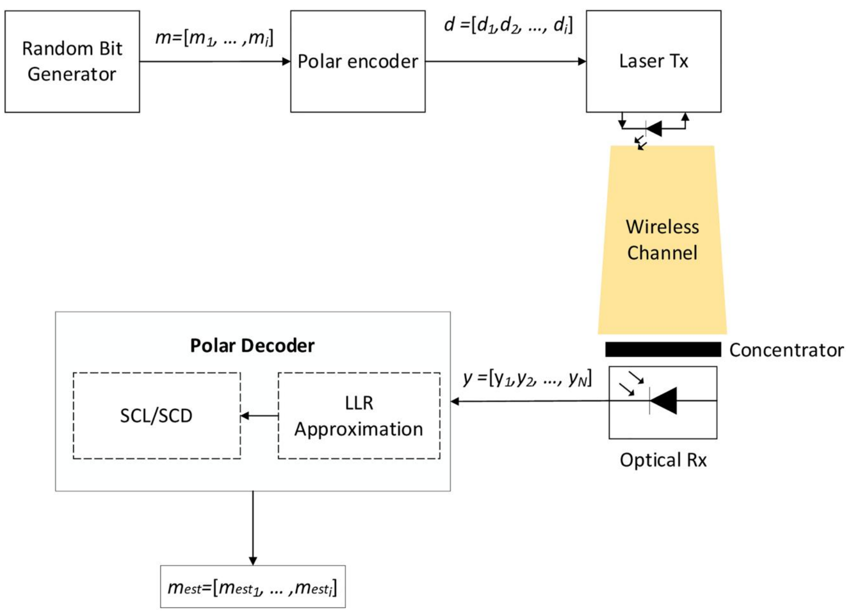

FIGURE 3 A system block diagram for the proposed scheme

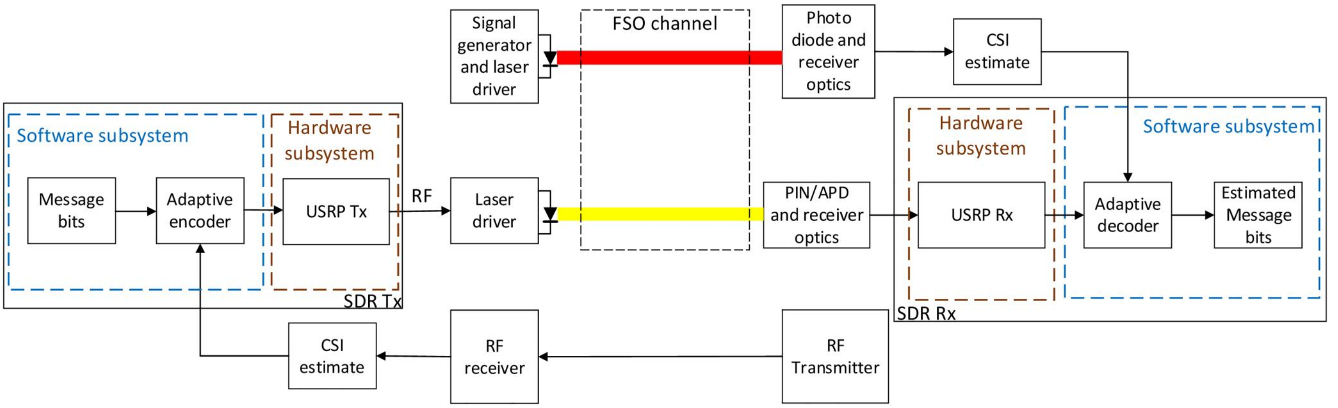

FIGURE 4 System block diagram for adaptive coding using software defined radio

the variance (scintillation index) of the fluctuating optical intensity of a modulated red laser transmitted from the receiver side. The resulting signal from the adaptive encoder is fed to the USRP transmitter which is modulated onto an RF carrier. The RF carrier is directly modulated and transmitted across the FSO channel using a laser driver.

3 | RESULTS AND DISCUSSION

3.1 | Software simulation results

The objective is to determine the optimum code rate for the weak turbulence regime, which maintains the BER at 10^{-9} with the 95% confidence limit for each scintillation index mentioned in Table 1. The amount the bits required with the 95% confidence limit is given by [45]

$$N_{\text{bits}} = \frac{-\ln(1 - \text{Confidence limit})}{\text{BER}}. \tag{24}$$

The OOK data stream, polar encoder, decoder, and the turbulence channel are implemented in C++. Using Monte-Carlo simulation, the optimum code rate under the weak and moderate turbulence regimes was determined utilising the system parameters provided in Table 1, and the results of the simulation are described in Table 2.

In each iteration, 1024-bit codewords are generated by the polar encoder as described in Section 2.1 for a specific R and transmitted over a LN/GG turbulence channel for a range of scintillation indices provided in Table 1. The received bit stream is decoded and the BER is evaluated $\frac{3\times10^6}{R}$ times to estimate the BER with a 95% confidence level. To determine the optimum R for each scenario, an initial R of 0.5 was used. The simulation was terminated, and R was decremented by 0.1–0.05 once the simulation reached 100 errors. The decrement in R depends on the number of iterations needed to reach 100 errors. It is to be noted that for each trial-and-error scenario, a total of N encoded bits were generated. If no errors were detected, R was incremented by 0.05.

TABLE 1 System parameters

Parameter	Value
Codeword length	1024
Iteration	$\frac{3\times10^6}{R}$
N_{bits}	3×10^9
BER confidence level	95%
Target BER	10^{-9}
Scintillation index σ_I^2	0.12, 0.2, 0.31

TABLE 2 Results of Monte-Carlo simulation

σ_I^2	Message bits transmitted	Message bits/frame	R
0.12	3×10^9	615	0.6
0.2	3×10^9	345	0.33
0.31	3×10^9	209	0.2

Based on Monte-Carlo simulation results, a performance comparison between SC and SCL decoders are demonstrated for $\sigma_I^2 = 0.12$, 0.2, and 0.31 in Figure 5a–c, respectively. In all turbulence scenarios, SCL with cyclic redundancy check (CRC) is adopted with a list size of 4, a CRC length of 11 [35], and N of 1024. Also, the plots for the link with no coding and turbulence are shown for reference. Under the turbulent condition, corruption of some bits allows for the message bits to be extracted from other uncorrupted bits. Because of this, FEC works above a certain SNR level. This tendency is more pronounced in capacity achieving codes such as Polar codes. Error propagation problem is severe with the occurrence of multiple bit errors at lower SNR. At higher SNR, as the occurrence of bit errors are reduced and therefore the performance in terms of coding is improved, that is, a sharp fall in the BER plots for the links with coding, which is depicted in Figure 5. In Figure 5a, for $\sigma_I^2 = 0.1$, the coding gain between uncoded OOK under turbulence with respect to the

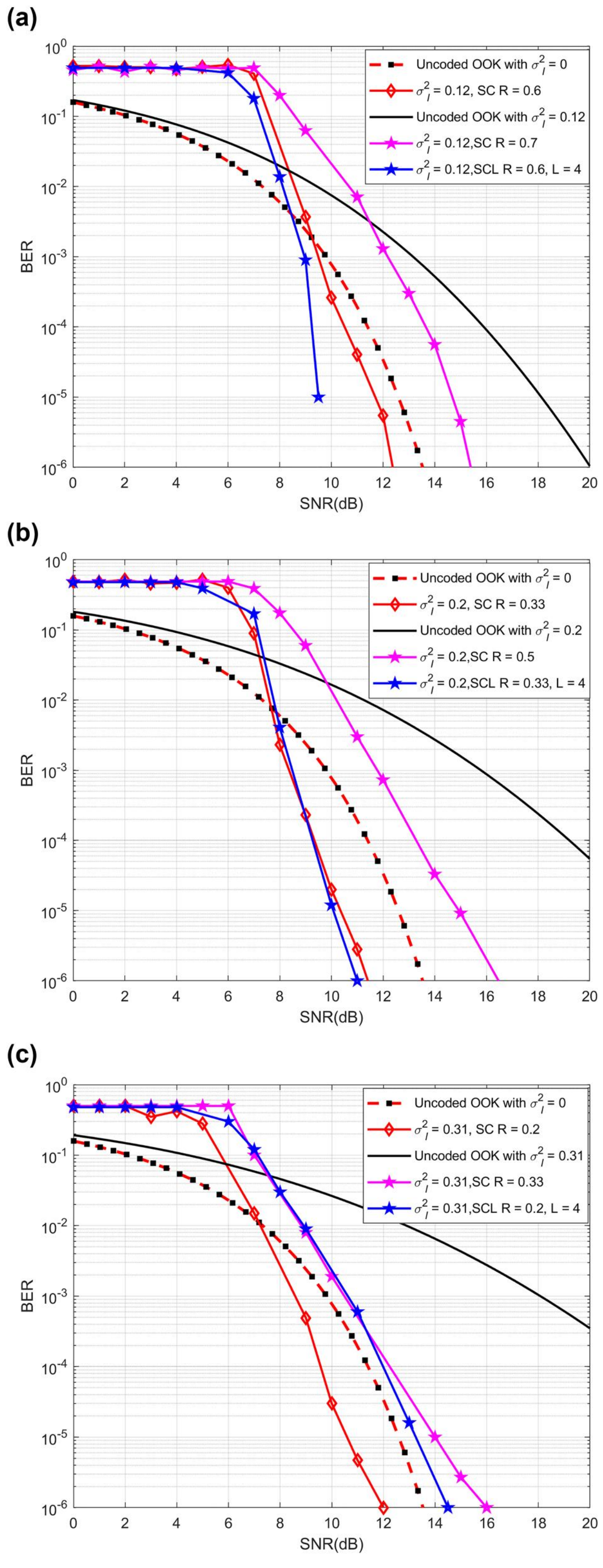

FIGURE 5 Bit error rate performance as a function of the SNR for the link with successive cancellation list (SCL) and SC decoders for σ_I^2: (a) 0.12, (b) 0.2, and (c) 0.31

SC decoder with $R = 0.6$ is 7 dB measured at the BER of 10^{-5}. The coding gain for the SC decoder with $R = 0.7$ is around 4 dB, which is 3 dB less than $R = 0.6$. SCL with $R = 0.6$ has improved performance with the coding gain of 6 dB, that is, 2.5 dB improvement over the SC decoder for the same R measured at the BER of 10^{-5}.

For $\sigma_I^2 = 0.2$, see Figure 5b, the coding gain of 10 dB is observed between uncoded OOK under turbulence and the SC decoder for $R = 0.33$. The SC decoder with $R = 0.5$ shows deteriorated performance compared with the case with $R = 0.33$ with a coding gain of 5 dB with respect to uncoded OOK under turbulence which is 5 dB worse off than $R = 0.33$ as measured at the BER of 10^{-4}. The SCL decoder has an improved performance with a coding gain of 10.3 dB with respect to uncoded OOK under turbulence, 0.3 dB improvement was observed over the SC decoder for the same R measured at BER of 10^{-6}.

For the case of $\sigma_I^2 = 0.31$ as shown in Figure 5c, the SC decoder with $R = 0.2$ has a coding gain of 13 dB with respect to the uncoded OOK under turbulence. The coding gain of 9 dB is observed for R of 0.3 with degradation of 4 dB compared with $R = 0.2$. Note, the SCL decoder offers lower performance compared with that of the SC decoder for the same R with a coding gain of 10 dB, that is, 2.5 dB lower than the SC decoder.

4 | CONCLUSION

This study investigated the robustness of polar codes in a FSO link under the weak turbulence regime assuming that the channel state information is not known at the receiver end. The log-likelihood ratio for OOK modulation was derived and based on the derivation the optimum R required to attain a confidence limit of 95% for the BER of 10^{-9} for scintillation indices 0.12, 0.2, and 0.31 were carried out using Monte-Carlo simulations. Comparisons between the SC and SCL decoders were drawn in which for σ_I^2 of 0.1 and 0.2, the SCL decoder offered coding gains of 2.5 and 0.3 dB, respectively, for the same R; for σ_I^2 of 0.3, the SC decoder demonstrated improved performance with a coding gain of 2.5 dB.

ACKNOWLEDGEMENT

This work is supported by Intensive Industrial Innovation Pprogram, Northeast, United Kingdom (IIIP NE)—25R17P01847, partly funded by the European regional development fund (ERDF), European Union's COST Action on Newfocus CA19111, and MEYS of the Czech Republic project LTC18008.

CONFLICT OF INTERESTS

The authors have no conflict of interest to declare.

DATA AVAILABILITY STATEMENT

Data available on request from the authors.

ORCID

Nithin Mohan https://orcid.org/0000-0003-2787-9900

REFERENCES

1. Uysal, M., et al.: Optical wireless communications, pp. 107–122. Springer, Switzerland (2016)
2. Cheng, M., Guo, L., Zhang, Y.: Scintillation and aperture averaging for Gaussian beams through non-Kolmogorov maritime atmospheric turbulence channels. Opt. Express. 23(25), 32606–32621 (2015). https://doi.org/10.1364/OE.23.032606
3. Perlot, N., Fritzsche, D.: Aperture averaging: theory and measurements. In: Free-Space Laser Communication Technologies XVI, vol. 5338, pp. 233–242. International Society for Optics and Photonics (2004)
4. Shen, H., Yu, L., Fan, C.: Temporal spectrum of atmospheric scintillation and the effects of aperture averaging and time averaging. Opt Commun. 330, 160–164 (2014)
5. Tsiftsis, T.A., et al.: FSO Links with spatial diversity over strong atmospheric turbulence channels. In: 2008 IEEE International Conference on Communications, 19-23 May, pp. 5379–5384 (2008). https://doi.org/10.1109/ICC.2008.1008
6. Yang, G., et al.: Contrasting space-time schemes for MIMO FSO systems with non-coherent modulation. In 2012 International Workshop on Optical Wireless Communications (IWOW), pp. 1–3. IEEE (2012)
7. Nor, N.A.M., et al.: Experimental investigation of all-optical relay-assisted 10 Gb/s FSO link over the atmospheric turbulence channel. J. Lightwave Technol. 35(1), 45–53 (2016)
8. Nor, N.A.M., et al.: Experimental analysis of a triple-hop relay-assisted FSO system with turbulence. Opt. Switch Netw. 33, 194–198 (2019)
9. Zhao, Z., Lyke, S.D., Roggemann, M.C.: Adaptive optical communication through turbulent atmospheric channels. In: 2008 IEEE International Conference on Communications, pp. 5432–5436. IEEE (2008)
10. Song, X., Cheng, J.: Subcarrier intensity modulated MIMO optical communications in atmospheric turbulence. J. Opt. Commun. Netw. 5(9), 1001–1009 (2013)
11. Safi, H., et al.: Adaptive channel coding and power control for practical FSO communication systems under channel estimation error. IEEE Trans. Veh. Technol. 68(8), 7566–7577 (2019)
12. Garcia-Zambrana, A.: Error rate performance for STBC in free-space optical communications through strong atmospheric turbulence. IEEE Commun. Lett. 11(5), 390–392 (2007)
13. García-Zambrana, A., Castillo-Vázquez, C., Castillo-Vázquez, B.: Rate-adaptive FSO links over atmospheric turbulence channels by jointly using repetition coding and silence periods. Opt. Express. 18(24), 25422–25440 (2010)
14. Pernice, R., et al.: Error mitigation using RaptorQ codes in an experimental indoor free space optical link under the influence of turbulence. IET Commun. 9(14), 1800–1806 (2015)
15. Zhou, H., Mao, S., Agrawal, P.: Optical power allocation for adaptive transmissions in wavelength-division multiplexing free space optical networks. Digit. Commun. Netw. 1(3), 171–180 (2015)
16. Djordjevic, I.B.: Adaptive modulation and coding for free-space optical channels. J. Opt. Commun. Netw. 2(5), 221–229 (2010)
17. Liu, L., Safari, M., Hranilovic, S.: Rate-adaptive FSO communication via rate-compatible punctured LDPC codes. In: 2013 IEEE International Conference on Communications (ICC), pp. 3948–3952. IEEE (2013)
18. Hassan, M.Z., et al.: Delay-QoS-aware adaptive modulation and power allocation for dual-channel coherent OWC. J. Opt. Commun. Netw. 10(3), 138–151 (2018)
19. Huang, Z., et al.: Computer-vision–based intelligent adaptive transmission for optical wireless communication. Opt. Express. 27(6), 7979–7987 (2019)
20. Blasco-Serrano, R., et al.: Polar codes for compress-and-forward in binary relay channels. In: 2010 Conference Record of the Forty Fourth Asilomar Conference on Signals, Systems and Computers, pp. 1743–1747. IEEE (2010)
21. Jouguet, P., Kunz-Jacques, S.: High performance error correction for quantum key distribution using polar codes. (2012). arXiv preprint arXiv:1204.5882
22. Fang, J., et al.: Performance investigation of the polar coded FSO communication system over turbulence channel. Appl. Opt. 57(25), 7378–7384 (2018)
23. Fang, J., et al.: Neural network decoder of polar codes with tanh-based modified LLR over FSO turbulence channel. Opt. Express. 28(2), 1679–1689 (2020)
24. Fang, J., et al.: Polar-coded MIMO FSO communication system over gamma-gamma turbulence channel with spatially correlated fading. J. Opt. Commun. Netw. 10(11), 915–923 (2018)
25. Tal, I., Vardy, A.: How to construct polar codes. IEEE Trans. Inf. Theor. 59(10), 6562–6582 (2013)
26. Lin, J., Yan, Z.: An efficient list decoder architecture for polar codes. IEEE Trans .Very Large Scale Integr. Syst. 23(11), 2508–2518 (2015)
27. Abadi, M.M., et al.: Implementation and evaluation of a gigabit Ethernet FSO link for the last metre and last mile access network. In: 2019 IEEE International Conference on Communications Workshops (ICC Workshops), pp. 1–6. IEEE (2019)
28. Khalighi, M., et al.: Turbulence mitigation by aperture averaging in wireless optical systems. In: 2009 10th International Conference on Telecommunications, pp. 59–66. IEEE (2009)
29. Rajbhandari, S., et al.: Experimental error performance of modulation schemes under a controlled laboratory turbulence FSO channel. J. Lightwave Technol. 33(1), 244–250 (2015)
30. Prokeš, A.: Modeling of atmospheric turbulence effect on terrestrial FSO link. Radioengineering. 18(1), 42–47 (2009)
31. Navidpour, S.M., Uysal, M., Kavehrad, M.: BER performance of free-space optical transmission with spatial diversity. IEEE Trans. Wirel. Commun. 6(8), 2813–2819 (2007)
32. Arikan, E.: Channel polarization: a method for constructing capacity-achieving codes for symmetric binary-input memoryless channels. IEEE Trans. Inf. Theor. 55(7), 3051–3073 (2009)
33. Bioglio, V., Condo, C., Land, I.: Design of polar codes in 5G new radio. IEEE Commun. Surv. Tutor. 23(1), 29–40 (2020)
34. Sarkis, G., et al.: Fast list decoders for polar codes. IEEE J. Sel. Area Commun. 34(2), 318–328 (2015)
35. Tal, I., Vardy, A.: List decoding of polar codes. IEEE Trans. Inf. Theor. 61(5), 2213–2226 (2015)
36. Condo, C., et al.: Design and implementation of a polar codes blind detection scheme. IEEE Trans. Circuits Syst. II. 66(6), 943–947 (2019). https://doi.org/10.1109/TCSII.2018.2872653
37. Le, D.-D., et al.: Log-likelihood ratio calculation using 3-bit soft-decision for error correction in visible light communication systems. IEICE Trans. Fund. Electron. Commun. Comput. Sci. 101(12), 2210–2212 (2018)
38. Olivatto, V.B., Lopes, R.R., de Lima, E.R.: Simplified method for log-likelihood ratio approximation in high-order modulations based on the Voronoi decomposition. IEEE Trans. Broadcast. 63(3), 583–589 (2017)
39. Olivatto, V.B., Lopes, R.R., de Lima, E.R.: Simplified LLR calculation for DVB-S2 LDPC decoder. In: 2015 IEEE International Conference on Communication, Networks and Satellite (COMNESTAT), pp. 26–31. IEEE (2015)
40. Park, J.W., et al.: Simplified soft-decision demapping algorithm for DVB-S2. In: 2009 International SoC Design Conference (ISOCC), pp. 444–447. IEEE (2009)
41. Yazdani, R., Ardakani, M.: Efficient LLR calculation for non-binary modulations over fading channels. IEEE Trans. Commun. 59(5), 1236–1241 (2011)

42. Ghassemlooy, Z., Popoola, W., Rajbhandari, S.: Optical wireless communications: system and channel modelling with Matlab®. CRC press (2019)
43. Mohan, N., et al.: Sectorised base stations for FSO ground-to-train communications. IET Optoelectron. 14(5), 312–318 (2020)
44. Kaur, P., Jain, V.K., Kar, S.: Performance of free space optical links in presence of turbulence, pointing errors and adverse weather conditions. Opt. Quant. Electron. 48(1), 65 (2016)
45. How Do I Measure the Bit Error Rate (BER) to a Given Confidence Level on the J-BERT M8020A and the M8040A High-Performance BERT? – Technical Support Knowledge Center Open, Edadocs.software.keysight.com, 2021. [Online]. https://edadocs.software.keysight.com/kkbopen/how-do-i-measure-the-bit-error-rate-ber-to-a-given-confidence-level-on-the-j-bert-m8020a-and-the-m8040a-high-performance-bert-588276182.html. [Accessed: 26 April 2021]

How to cite this article: Mohan, N., et al.: The BER performance of a FSO system with polar codes under weak turbulence. IET Opotelectron. 1–9 (2021). https://doi.org/10.1049/ote2.12058